Structural Analyses of the Cold Mass for High Field Dusty Plasma Experiment

Craig E. Miller, Alexey Radovinsky, and Shahin Pourrahimi

***Abstract*—A magnet to study the properties of dusty plasmas in the presence of a magnetic field has been proposed. This magnet has four operating modes to vary the experimental test region and target magnetic field values. The design of the cold mass for the high field magnetized dusty plasma experiment is presented and analyzed. The cold mass includes four coils, ground insulation covering the winding packs, and coil cases used to safely support the coils. Dimensions of the four coils are specified by the magnetic design, and the equipment used to view the dusty plasma apply spatial constraints to the cold mass design. The design also considers the manufacturing process for the cold mass and the stresses resulting from electromagnetic loads coupled with thermal loads. Only one operating mode is considered in this analysis as the others produce significantly lower electromagnetic forces. Resulting stresses compare favorably to failure criteria at critical locations.**

***Index Terms*—Cold mass design, dusty plasma experiment, finite element analysis (FEA), superconducting magnet.**

I. Introduction

THE MAGNET used for the dusty plasma experiment is considered high field and high precision and it is capable of operation in four different modes to achieve various physics goals. For example, the first operating mode has a 4 T field and $< 1\%$ uniformity along a 5 cm extent of the centerline. The design of the cold mass for the high field dusty plasma is created around two constraints: (1) the dimensions of four superconducting (SC) coils from the magnetic design at 4 K, and (2) the outer dimensions of the cryostat specified by laboratory space and plasma viewing system.

II. Mechanical Design

Fig. 1 shows the nominal outer dimensions of the cryostat. The 50 cm inner diameter is critical for the chamber containing the plasma under study. The plasma is observed through four viewports extending across the outer diameter of the cryostat and along the mid-plane. Each view port requires 15 cm lateral clearance and 20 cm axial clearance as shown in Fig. 1.

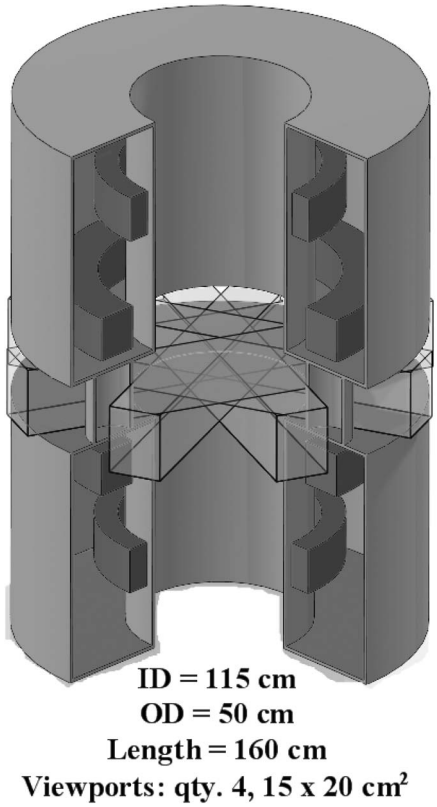

Fig. 1. Dimensions of the cryostat allowing for 50 cm diameter chamber along magnet centerline and transparent viewports on midplane. Four SC coils are shown within cryostat.

The geometry used to analyze the structural integrity of the cold mass is shown in Fig. 2. The full geometry is reduced to 1/8th of its entirety via symmetry about the mid-plane and four-fold symmetry around the central axis. In the analysis, boundary conditions are applied to all areas lying on planes of symmetry to account for the structure that is not included. Notice there is no coil case along the inside diameter of Coil #1. This is because there is not sufficient clearance between the inside of the coil and the cryostat to include a structural member. The structural support of the coils consists of a coil case for each coil connected via four I-Beams and four posts.

The coil case consists of aluminum 6061-T6 alloy and stainless steel in order to match the orthotropic thermal expansion of the winding pack. The vertical portions of the coil case are aluminum, which secures the coils via epoxy bonding. The aluminum alloy matches the axial thermal contraction of the coil closely and provides a good thermal conduction path to the coil. Stainless steel is used on the horizontal portions of the coil case

Manuscript received July 17, 2013; accepted September 29, 2013. Date of publication October 9, 2013; date of current version November 9, 2013. This work was supported in part by Subagreement 11-PHYS-200373-MIT from Auburn University (prime sponsor NSF).

C. E. Miller and A. Radovinsky are with Plasma Science and Fusion Center, Massachusetts Institute of Technology (MIT), Cambridge, MA 02139 USA (e-mail: cemiller@psfc.mit.edu; radovinsky@psfc.mit.edu).

S. Pourrahimi is with Superconducting Systems Inc., Billerica, MA 01821 USA (e-mail: Pourrahimi@ssi99.com).

Color versions of one or more of the figures in this paper are available online at http://ieeexplore.ieee.org.

Digital Object Identifier 10.1109/TASC.2013.2285092

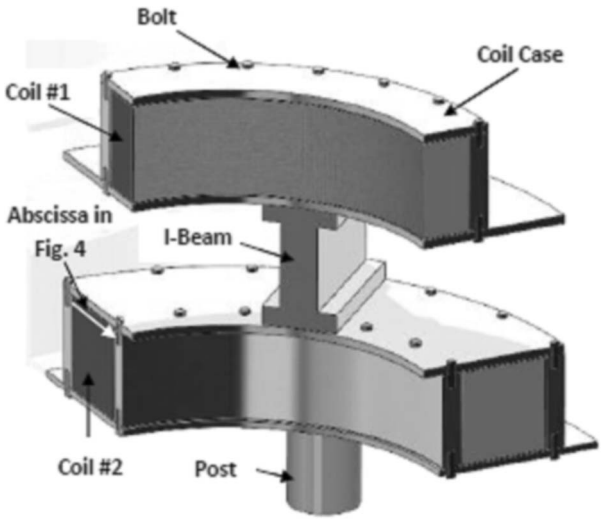

Fig. 2. Reduced model used for the structural analysis of magnet. Notice the abscissa for the graph plotted in Fig. 4.

and provides sufficient stiffness to prevent field errors due to axial bending of the structure.

The metallic coil case consists of aluminum 6061-T6 and stainless steel and is bolted together around the coils. In the FEA model an I-beam is used between Coil #1 and Coil #2 to support the large vertical load as well as the bending moment created by the coils having different diameters. A cylindrical post is used through the mid-plane connecting Coil #2 and Coil #3 (not shown in Fig. 2 as it is excluded via symmetry).

All coils are electrically isolated with fiberglass ground insulation. It is assumed the fiberglass is well bonded to the winding pack. The vertical surface on the outside diameter of the ground insulation and the coil case are bonded together. The horizontal interfaces between the ground insulation and the coil case can either be bonded or allow sliding. One purpose of the structural analyses is to determine how these contact conditions affect the stress distributions.

III. Material Properties

Three types of material behavior are used in these analyses: (1) isotropic, (2) transversely isotropic, and (3) orthotropic. The isotropic materials are aluminum 6061-T6 alloy and stainless steel and their temperature dependent material properties are used. Fiberglass material is used for the ground insulation and is assumed to be transversely isotropic, meaning it is isotropic in-plane and has different material properties through its thickness as described in [1]. Tables I and II summarize the properties used in the analyses for the isotropic and transversely isotropic materials, respectively.

The winding pack has too many details to describe fully in these three-dimensional simulations. Therefore, the coil is reduced to orthotropic material properties that use values averaged, or smeared, through its volume. Coordinate systems are assigned to the coil to orient its material properties with the winding direction.

In order to determine the orthotropic material properties of a coil, two methods are implemented. First, in the direction of the winding, material properties are calculated from standard rule-of-mixtures formulas [2]. These formulas determine smeared values based upon constituent values and weigh them based upon % of cross-sectional area each constituent represents. Table I includes material properties for the copper, SC wire and epoxy constituents of the coils. Second, the in-plane material properties are determined using a detailed two-dimensional (2D) Finite Element Analysis (FEA) model of a portion of the winding pack shown in Fig. 3.

Smeared elastic moduli are determined by applying displacements on opposite edges of the structure and calculating the load reactions. This is shown in the vertical direction in Fig. 3 and is repeated in the horizontal direction and repeated again at various temperatures. The load versus displacement data are used to calculate temperature dependent elastic moduli in orthogonal directions.

Smeared thermal expansion coefficients are determined by applying uniform temperature and placing boundary conditions

TABLE I
Temperature-Dependent Material Properties Used in FEA for Isotropic Materials

Material	Temperature (K)	Secant CTE (10^{-6}/K)	Elastic Modulus (10^9 Pa)	Poisson's Ratio
Copper	295	11.4 [4]	129 [5]	0.31 [5]
	4	0	138 [5]	
St. Steel 316LN	295	10.3 [4]	194 [4]	0.25 [6]
	4	0	205 [4]	
Aluminum 6061-T6	295	14.4 [7]	71.8 [8],[9]	0.33 [6]
	4	0	80.9 [8],[9]	
SC Wire	295	11.3 [4]	90 [10],[11]	0.33
	4	0	80 [10],[11]	
Epoxy/ Formvar	295	55 [4]	2.6 [10],[11]	0.4
	4	0	7.4 [10],[11]	

TABLE II
Temperature-Dependent Material Properties Used in FEA for Orthotropic and Transversely Isotropic Materials

Material	Temperature (K)	Secant CTE (10^{-6}/K)	Elastic Modulus (10^9 Pa)	Poisson's Ratio
Smeared Coil - Hoop	295	10.4	90.2	0.31
	4	0	103	
Smeared Coil - Radial	295	13.4	18.9	0.25
	4	0	38.6	
Smeared Coil - Axial	295	14.1	19.5	0.37
	4	0	19.5	
G-10CR in-plane	295	8.32 [4]	22 [10],[11]	0.36 [12]
	4	0	27 [10],[11]	0.25 [12]
G-10CR normal	295	24.4 [4]	14 [10],[11]	0.25 [12]
	4	0	22 [10],[11]	0.15 [12]

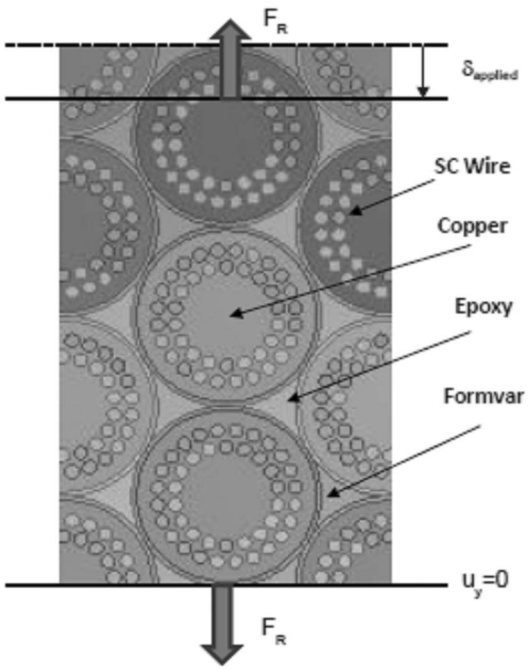

Fig. 3. Detailed geometry of winding pack used for 2D FEA to obtain material properties.

on the model to prevent rigid body motion. Resulting average displacements along the edges shown were calculated to determine the temperature dependent axial and radial thermal expansion coefficients reported in Table II.

IV. Analysis

There are two sets of parameters used for the analyses presented: (1) the applied loads, and (2) the contact condition between the coil and the coil case. First, the loads applied to the cold mass are either: (i) cool down to 4 K, or (ii) cool down to 4 K plus Electromagnetic (EM) loads. The second variable is the contact condition between the horizontal surfaces (shoulders) of all coils and the coil case. These surfaces at the fiberglass to coil case interface are either: (i) bonded, or (ii) able to slide with $\mu = 0.1$, where μ is the friction coefficient. The value of $\mu = 0.1$ is at the low end of typical values and assumes some lubricant is applied between the ground insulation and coil case [3].

Bolts are not explicitly included in the model, but are considered using bolt pretension loads on surfaces bolts interact with the structure. The Magneto-static module of the Maxwell software is used to calculate the EM [Lorentz] forces by applying a 103 A/mm^2 current density to both coils. The peak magnetic flux of 6.7 T is located at the inside of Coil #2. The finite element program ANSYS is used to apply all loads, calculate all displacement and stress fields, and quantify fiberglass integrity used to evaluate the cold mass.

A. Winding Pack Stresses

The shear stresses on the surface of the winding pack act through the thickness of the ground insulation between the coil case and the winding pack. It is the shear stress that is a significant factor in the decision between bonding or allowing sliding between the winding pack and the horizontal components of the coil case.

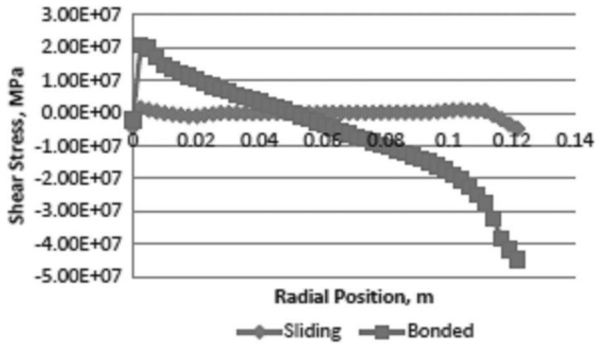

Fig. 4. Shear stress on top surface of ground insulation for sliding and bonded coils at 4 K with EM loads applied.

Fig. 4 plots the shear stresses in the fiberglass at the top of Coil #2 along the line shown in Fig. 2. The shear stresses are plotted for the cases of bonded and frictional contact at 4 K and EM loads. The case where the coil shoulders are bonded to the coil leads to very high shear stresses through the ground insulation. At 4 K, the shear stress reached 20 MPa and at 4 K + EM loads, the shear stresses reach 45 MPa as seen in Fig. 4. This high level of stress combined with their location at the edge of the structure will most likely propagate any cracks that form, leading to a loss of structural integrity. In the case where sliding is allowed, there are low levels of shear, up to 5 MPa as seen in Fig. 4.

As previously discussed, the coil is comprised of copper, SC wires and epoxy. Comparing the resulting stresses to failure criteria is complicated because of the variety of materials comprising the winding pack. A conservative approach is to assume the copper carries all loads within the coil. The hoop stress, σ_{hoop}, in the copper is calculated by scaling the hoop strains, $\varepsilon_{\mathrm{hoop}}$, by the elastic modulus of copper, $\mathrm{E_{cop}}$. For the case of sliding coils at 4 K with EM loads, this approach yields: $\sigma_{\mathrm{hoop}} = \varepsilon_{\mathrm{hoop}} * \mathrm{E_{cop}} = 0.12\% * 138$ GPa $= 169$ MPa in tension, which is much lower than the 270 MPa copper failure criteria.

B. Displacements

The displacements are of interest for several reasons. First, the coil position creates the desired magnetic flux distribution and displacements should be minimized. Second, there will be tight clearances between the cryostat, shield and coil support and we want to prevent the displacements during cool-down and coil charging from closing any initial gaps between the parts. Third, the effect of the contraction of the entire structure is incorporated into the room temperature dimensions. Typically the magnetic design specifies the dimensions of the coils at 4 K, whereas all components are fabricated at room temperature. Therefore, the calculated displacements must be added to the 4 K dimensions for the manufacturing drawings. Fourth, the radial displacements indicate the amount of clearance necessary to include between the aluminum and stainless steel parts of the coil case. Such clearances are necessary because of the

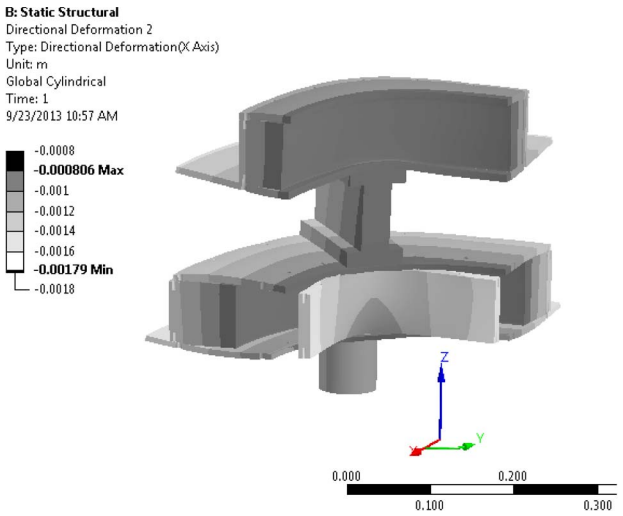

Fig. 5. Radial displacement contour plotted on deformed structure (magnified 85× to aid visualization). Inner aluminum moves 1.8 mm from stainless steel and clearances must be included in detailed design.

differential thermal contraction. If no clearances are included then the differential contraction will be absorbed by the bolts, and lead to shear failure of the bolts. Fifth, the displacement maps can provide a visualization of the root cause of stresses.

Fig. 5 shows a contour map of the radial displacement on the cold mass surface for the case of 4 K and EM loads with sliding between the coil and coil case. The model shape is deformed using a 100× magnification factor. Notice the deflection of the inner aluminum component of the coil case away from Coil #2. The 1.8 mm of deflection and must be included as clearance in the bolt holes connecting the aluminum component. Also, notice the relatively small changes in axial displacement around the coils along the azimuthal direction, so field errors due to coil deformation is not expected.

V. Conclusion

The structural design for the cold mass of the dusty plasma magnet has been analyzed. All loads are safely carried by the structure when sliding is allowed between the horizontal surfaces of the coils and the coil case. It is recommended to experimentally test bolting stainless steel to aluminum at these dimensions to observe if necessary sliding occurs to prevent failure of the bolts. This design is ready to proceed to the detailed design stage of the project.

References

[1] C. E. Miller and A. Radovinsky, "Structural analyses of the JLab Hall D replacement solenoid," *IEEE Trans. Appl. Supercond.*, vol. 23, no. 3, p. 4900304, Jun. 2013.
[2] [Online]. Available: http://en.wikipedia.org/wiki/Rule_of_mixtures
[3] E. L. Stone and W. C. Young, "Coefficient of friction measurements of fiberglass/epoxy at cryogenic temperatures," in *Proc. Adv. Cryogenic Eng.*, 1980, vol. 26, pp. 315–318.
[4] [Online]. Available: http://cryogenics.nist.gov/MPropsMAY/material%20properties.htm
[5] N. J. Simon, E. Drexler, and R. Reed, "Properties of copper and copper alloys at cryogenic temperatures," Nat. Inst. Standards Technol. (NIST), Gaithersburg, MD, USA, NIST Monogr. 177, Feb. 1992.
[6] [Online]. Available: www.matweb.com
[7] Y. Iwasa, *Case Studies in Superconducting Magnets*. New York, NY, USA: Springer-Verlag, 2009, p. 638.
[8] M. Fink, T. Fabing, M. Scheerer, E. Semerad, and B. Dunn, "Measurement of mechanical properties of electronic materials at temperatures down to 4.2 K," *Cryogenics*, vol. 48, no. 11/12, pp. 497–510, Nov./Dec. 2008.
[9] D. T. Read and H. M. Ledbetter, "Temperature dependence of the elastic constants of an NbTi/Cu superconducting composite," *Composites*, vol. 9, no. 4, pp. 100–104, Apr. 1978.
[10] R. P. Reed and A. F. Cark, *Material at Low Temperatures*. Materials Park, OH, USA: ASM, 1983.
[11] Y. Shindo, K. Horiguchi, and R. Wang, "Cryomechanics and short-beam interlaminar shear strength of G-10CR glass-cloth/epoxy laminates," in *Proc. Adv. Cryogenic Eng.*, 2000, vol. 46A, pp. 167–174.
[12] M. B. Kasen, G. R. MacDonald, D. H. Beekman, Jr., and R. E. Schramm, "Mechanical, electrical and thermal characterization of G-10CR and G-11CR glass-cloth/epoxy laminates between room temperature and 4 K," in *Proc. Adv. Cryogenic Eng.*, 1981, vol. 26, pp. 235–244.